CrystEngComm

Dynamic Article Links

Cite this: *CrystEngComm*, 2012, **14**, 1665

www.rsc.org/crystengcomm

PAPER

The influence of dislocations on optical and electrical properties of epitaxial ZnO on Si (111) using a γ-Al_2O_3 buffer layer

W.-R. Liu,[ab] B. H. Lin,[ac] S. Yang,[c] C. C. Kuo,[c] Y.-H. Li,[c] C.-H. Hsu,*[ac] W. F. Hsieh,*[ac] W. C. Lee,[d] M. Hong[d] and J. Kwo[ef]

Received 17th September 2011, Accepted 2nd December 2011
DOI: 10.1039/c2ce06218f

The structural, optical and electrical properties of the *c*-plane ZnO epitaxial films grown by pulsed laser deposition on a Si(111) substrate buffered with a thin layer of γ-Al_2O_3 were investigated by X-ray diffraction, transmission electron microscopy, photoluminescence (PL) and Hall measurements. Detailed structural investigation showed that the dominant structural defects in the ZnO films are threading dislocations (TDs). Experimental results manifest the edge- and screw-type of TDs influence the optical and electric properties differently; the intensity ratio between the PL yellow-green band to near band edge emission and the carrier concentration are affected mainly by the edge TD, and the FWHM of the near band edge emission is dominantly influenced by the screw TD.

Introduction

ZnO, a II–VI compound semiconductor, is a promising material for highly efficient light-emitting devices and other optical applications for UV luminescence because of its wide direct band gap, 3.37 eV, and large exciton binding energy, 60 meV near 295 K.[1] Much attention has been given to grow an epitaxial ZnO film on a silicon substrate because of the unique opportunity of integrating optoelectronic devices in the UV region with well developed Si technology, but the growth of a ZnO epitaxial film directly on Si(111) is a great challenge because of the large mismatch of lattice parameter (15%) and thermal expansion coefficient (56%). More importantly, the formation of an amorphous SiO_2 layer at the ZnO/Si(111) interface prohibits the formation of a high-quality epitaxial layer and results in polycrystalline or highly textured ZnO films.[2–4] Much effort has therefore been devoted to grow a (0001)-oriented ZnO epitaxial film with various buffer layers, such as γ-Al_2O_3,[5] Y_2O_3,[6] ZnS,[2] Zn/MgO,[7] Mg/MgO,[8] Sc_2O_3[9] and GaN.[10]

Structural defects, such as threading dislocations (TDs), are inevitably generated inside the ZnO layer at a large density to release the strain energy caused by the large lattice mismatch and the significant difference in thermal expansion coefficient between ZnO and the substrate. A dislocation is well known to serve as a sink of point defects; it produces defect states in the band gap, which enhance the deep-level emission (DLE) in photoluminescence (PL) spectra and can be partially occupied by negative charges until the energy of the states attains the Fermi energy of ZnO.[11–15] The type and geometry of dislocations thus crucially affect the electrical and optical properties of the ZnO epi-films.

In this work, we investigated the influence of various TDs on PL and the carrier concentration of a high-quality ZnO epi-film grown on a Si(111) substrate buffered with a γ-Al_2O_3 epi-layer of thickness 15 nm. The decreased enthalpy of formation of γ-Al_2O_3 ($\Delta H_{\gamma\text{-}Al2O3} = -1643.7$ kJ mol^{-1}) relative to SiO_2 ($\Delta H_{SiO2} = -910$ kJ mol^{-1}) impedes the formation of interfacial silica and results in the epitaxial growth of γ-Al_2O_3 on Si.[5] The density of TDs and the crystal structure were analyzed with X-ray diffraction (XRD) and a transmission electron microscope (TEM). PL and the Hall effect were measured to characterize the optical and electrical properties, which exhibit a strong correlation with the edge and screw TDs but in varied aspects.

Experimental

A cubic γ-Al_2O_3 (a_0 = 7.911 Å) of thickness ~15 nm was deposited on a Si(111) substrate near 750 °C using electron-beam evaporation from a highly pure single-crystal sapphire source in a multi-chamber molecular-beam-epitaxy (MBE) growth system.[16] The details of the growth of the γ-Al_2O_3 epi-layer are reported elsewhere.[17] The ZnO layers of thickness ~0.3 μm were subsequently grown by deposition with a pulsed KrF excimer laser (PLD) (λ = 248 nm).[5,6] The beam was focused to produce an

[a]*Division of Scientific Research, National Synchrotron Radiation Research Center, Hsinchu, 30076, Taiwan. E-mail: chsu@nsrrc.org.tw; wfhsieh@mail.nctu.edu.tw*
[b]*Department of Photonics & Institute of Electro-Optical Science and Engineering, National Cheng Kung University, Tainan, 70101, Taiwan*
[c]*Department of Photonics and Institute of Electro-Optical Engineering National Chiao Tung University, Hsinchu, 30010, Taiwan*
[d]*Department of Materials Science & Engineering, National Tsing Hua University, Hsinchu, 30013, Taiwan*
[e]*Center for Condensed Matter Sciences, National Taiwan University, Taipei, 10617, Taiwan*
[f]*Department of Physics, National Tsing Hua University, Hsinchu, 30013, Taiwan*

This journal is © The Royal Society of Chemistry 2012

energy density of 5–7 J cm^{-2} at a repetition rate of 10 Hz on a commercial hot-pressed stoichiometric ZnO (5N) target. No oxygen gas flow was introduced during growth, and the substrate temperature ranged from 200 to 400 °C. The structural properties of the samples were characterized with XRD and TEM. XRD measurements were performed with a four-circle diffractometer at beamline BL13A of National Synchrotron Radiation Research Center (NSRRC), Taiwan with an incident wavelength of 1.0247 Å. Slits in two pairs were located between the sample and a NaI scintillation detector to yield a resolution typically better than 4×10^{-3} nm^{-1}. Cross-sectional TEM images were recorded (by MA Tech) with a TEM (field-emission-gun type, Philips TECNAI-20). The electrical properties were characterized with a Hall measurement system (Ecopia HMS-3000) in a van der Pauw configuration at 295 K. The PL was measured with a He–Cd laser (wavelength 325 nm) as a pumping source. The emitted light was dispersed with a spectrometer (Triax-320) and detected with a photomultiplier tube sensitive to UV light.

Results and discussion

A cross-sectional TEM image of a sample grown at 300 °C with a Si [10$\bar{1}$] pole is shown in Fig. 1, which illustrates the great crystalline quality of the grown layers and the sharp γ-Al_2O_3/Si interface. No amorphous interfacial layer was found. The selected-area electron-diffraction (SAED) pattern recorded near the buffer region, as depicted in the inset of Fig. 1, reveals the epitaxial relation of ZnO(0001)‖γ-Al_2O_3(111)‖Si(111) and ZnO⟨10$\bar{1}$0⟩‖Si⟨11$\bar{2}$⟩, but the observation of two 040 reflections of γ-Al_2O_3 in the SAED pattern is contrary to the expected three-fold symmetry. Previous X-ray scattering measurements showed that the growth of γ-Al_2O_3 on Si(111) conformed to a cube-on-cube growth with its (111) planes parallel to the Si substrate surface.[17] Azimuthally, two rotational twins coexist with the A-type domains of γ-Al_2O_3[2$\bar{1}\bar{1}$]‖Si[2$\bar{1}\bar{1}$] dominating over the B-type domains of γ-Al_2O_3[2$\bar{1}\bar{1}$]‖Si[$\bar{2}$11], as evident from the XRD ϕ-scans across Si 220 and γ-Al_2O_3 440 reflections, depicted in Fig. 2. Also displayed at the bottom of Fig. 2 is an azimuthal scan across ZnO 10$\bar{1}$1 reflections; six evenly spaced sharp peaks elucidate the hexagonal symmetry of wurtzite ZnO. The coincidence of the angular positions of these peaks with those of γ-Al_2O_3 440 yields an epitaxial relation of ZnO (0001)⟨10$\bar{1}$0⟩‖γ-Al_2O_3 (111)⟨11$\bar{2}$⟩. Fig. 2 shows also that the width of the peaks of azimuthal scans across ZnO off-normal reflections is one half to one third of that of the underlying γ-Al_2O_3. The lateral coherent length of ZnO is more than ten times that of the γ-Al_2O_3 buffer layer as determined by the XRD in-plane radial scans (not shown). The structural characteristics of the ZnO layer are clearly superior to those of the γ-Al_2O_3 buffer layer. A large density of defects is expected near the interfacial region to accommodate the lattice deformation, as evident from the progressive improvement of ZnO crystalline perfection with increasing layer thickness.

The crystal structure of γ-Al_2O_3 belongs to space group $Fd\bar{3}m$ (space group number 227) with oxygen atoms occupying the 32*e* sites (Wyckoff positions). Along the [111] direction, each unit cell contains six oxygen layers, nearly equally spaced, in which oxygen atoms form a 2-D defective hexagonal lattice as illustrated in Fig. 3. The stacking of the oxygen layers follows a sequence A–B–C–A–B–C along [111], resembling a face-centered cubic (fcc) lattice. According to the determined epitaxial relation, the unit cell of ZnO, depicted as a red shaded parallelogram, is aligned with the oxygen sub-lattice in γ-Al_2O_3, the blue parallelogram. An identical orientation relation has been observed in ZnO grown on various oxide surfaces including sapphire(0001),[16,18] Y_2O_3(111),[6] $Gd_2O_3(Ga_2O_3)$(111)[19] and La_2O_3(111).[20] This observation strongly indicates that the continuity of the oxygen sub-lattice anchors the orientation of the ZnO overlayer.

The lattice parameter $a = 3.24$ Å of ZnO ($c = 5.20$ Å) is about 16% larger than the lattice parameter of the hexagonal oxygen sub-lattice in γ-Al_2O_3, $a(\mathrm{O}) = \sqrt{2}/4 \times a_0(\gamma - Al_2O_3) = 2.80$ Å. According to a picture of epitaxial growth, the ZnO layer was expected to be compressively strained, but the large lattice mismatch was readily accommodated during the early stage of growth through the generation of misfit dislocations at a large density near the γ-Al_2O_3/ZnO interface. The abrupt diminution of the strain field can be visualized according to the contrast variation localized near the γ-Al_2O_3/ZnO interface in the cross-section TEM micrograph shown at small magnification in

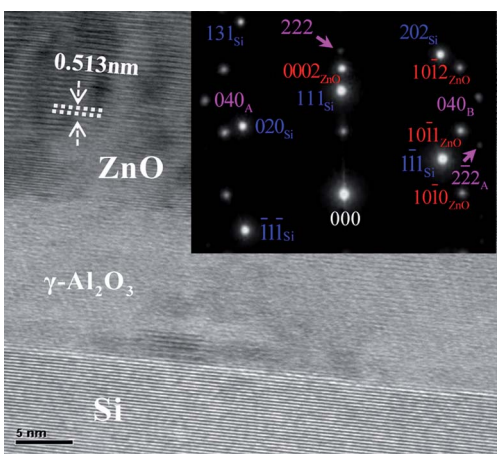

Fig. 1 Cross-sectional TEM micrograph recorded along projection $[10\bar{1}]_{Si}$ and the corresponding SAED pattern in the inset. Subscripts A and B denote the rotational domain of γ-Al_2O_3 aligned and rotated 180° with the Si lattice, respectively.

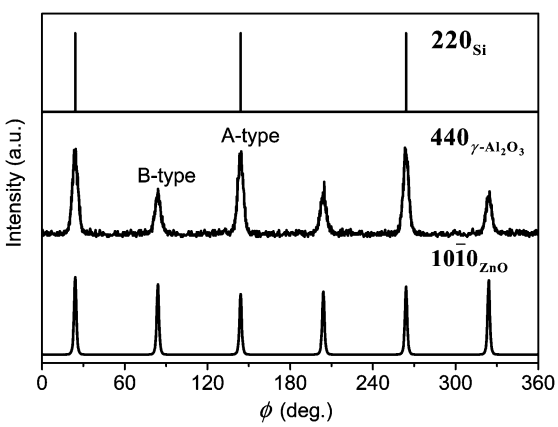

Fig. 2 XRD azimuthal scans across off-normal ZnO 10$\bar{1}$1, γ-Al_2O_3 440, and Si 220 reflections.

This journal is © The Royal Society of Chemistry 2012

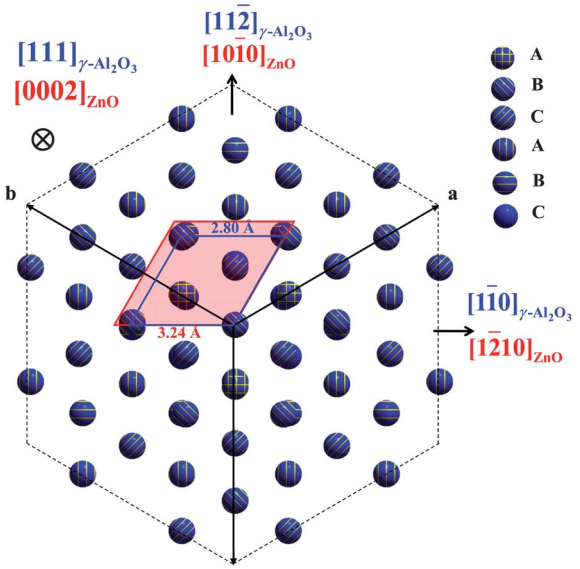

Fig. 3 Projection of the oxygen sub-lattice onto the γ-Al_2O_3 (111) surface. The smaller parallelogram depicts the corresponding 2-D hexagonal unit cell and the larger one is the unit cell of ZnO in the basal plane. A, B, and C indicate the O^{2-} ionic position of a stacking sequence along the [111] direction in the γ-Al_2O_3 unit cell.

Fig. 4. All ZnO layers of our samples exhibited a lateral lattice parameter (within ~0.3%) slightly larger than the bulk value as determined by XRD data. The ZnO layers were hence fully relaxed at that growth temperature, and the observed tensile strain state is attributed to the coefficient of thermal expansion of ZnO (5.0×10^{-6} K^{-1}) being larger than that of Si (3.6×10^{-6} K^{-1}), which would produce a tensile thermal stress. Even though γ-Al_2O_3 has the largest thermal expansion coefficient (8.2×10^{-6} K^{-1}) among the three materials, the thermal stress induced by the γ-Al_2O_3 layer is negligible in this case because of its slight thickness. We observed the same phenomenon in other ZnO/Si(111) hetero-epitaxial systems with various buffer layers of nanometre thickness, such as Y_2O_3[6] and $Gd_2O_3(Ga_2O_3)$.[19]

In addition to misfit dislocations, there also exist threading dislocations (TDs) running through the interior of the ZnO layers primarily along the [0001] direction, similar to what was found in ZnO films grown on commonly used *c*-sapphire.[16] These TDs are identified by the contrast lines stemming from the ZnO/γ-Al_2O_3 interface in Fig. 4. Dislocations are classified into three types—screw, edge and mixed, according to the direction of the corresponding Burgers vector (***b***) relative to the dislocation line

Fig. 4 Bright-field cross-section TEM image of the ZnO film grown at 300 °C under two-beam conditions with $g = 0002$, at small magnification.

direction.[21,22] For a (0001)-oriented thin film of wurtzite structure, with the TDs with their dislocation lines lying along the [0001] direction, the Burgers vectors ***b*** of edge, screw and mixed dislocations are, respectively, $\boldsymbol{b}_C = \langle 0001 \rangle$, $\boldsymbol{b}_E = 1/3\langle 11\bar{2}0 \rangle$ and $\boldsymbol{b}_M = 1/3\langle 11\bar{2}3 \rangle$, which is a combination of $\boldsymbol{b}_C$ and $\boldsymbol{b}_E$. The type of dislocations can be characterized with a TEM diffraction-contrast analysis. The contrast of dislocations in TEM images arises from diffraction on the lattice planes that are distorted by the dislocations. Applying the invisibility criterion $\boldsymbol{g}\cdot\boldsymbol{b} = 0$,[23,24] in which ***g*** denotes the operating diffraction vector, we analyzed the images of the sample grown at 300 °C recorded with ***g*** equal to ZnO 0002, $11\bar{2}0$, and $11\bar{2}2$ reciprocal lattice vectors. The total density of TDs is determined to be approximately 2.4×10^{10} cm^{-2} and the edge component prevails over the screw component.

To assess quantitatively the defect structures, we performed XRD measurements. Edge TDs have the corresponding Burgers vector lying in the basal plane of ZnO; they twist the surrounding lattice about the *c*-axis and lead to the formation of vertical grain boundaries.[22,25,26] In contrast, screw TDs have the corresponding Burgers vector parallel to the *c*-axis; they tilt the ZnO lattice, generate a pure shear strain field[27] and deform the basal planes. The $(h0\bar{h}0)$ crystalline planes are thus distorted by the edge TD but are unaffected by the screw TD; the associated profiles thus serve to determine the twist angle and the density of edge dislocations. In contrast, the $000l$ reflections are sensitive to screw but not to edge TDs; their line widths are employed to determine the tilt angle and the density of screw TDs in ZnO.

The $h0\bar{h}0$ and $000l$ reflections were measured to investigate the influence of the edge and screw TD, respectively. The full width at half maximum (FWHM) of $h0\bar{h}0$ and $000l$ rocking curves reflect the lattice twist or tilt, and the line widths of radial scans yield the lateral or vertical inhomogeneous strain field and domain size. We employed the Williamson–Hall (W–H) plot (Δq *vs.* q, in which $q = 4\pi\sin\theta/\lambda$ denotes the scattering vector and Δq is the line width of q along the radial direction) to analyze the line width of radial scans, to separate the reflection profile broadening due to a finite structural coherent length from the strain-induced broadening. The inverse of the ordinate intercept yields the coherence length, or equivalently the effective domain size; the slope yields the root-mean-square inhomogeneous strain averaged over the effective domains.[28] The coherence lengths and inhomogeneous strains along the in-plane and growth directions with the tilt and twist angles of the samples grown at various temperatures are listed in Table 1. The range of the structural coherence lengths in both directions is a few thousand Å. For samples grown at 200 and 300 °C, the coherence length along the growth direction is comparable with the layer thickness, implying that the structure retains coherence throughout the entire layer thickness. The average lateral strain is 3.4–4.7 $\times 10^{-3}$, about 2–3 times that along the surface normal, 1.3 to 1.6 $\times 10^{-3}$. The twist angle (α_Φ) and tilt angle (α_Ω) of ZnO fall in ranges 1.63–1.89° and 0.34–0.51°, respectively. The ZnO layer with the least tilt angle thus has the largest twist angle. The same trend was observed in samples of another batch grown under the same conditions but on a buffer layer with slightly poorer structural perfection. This phenomenon was not observed, however, for ZnO grown on other buffer layers, such as Y_2O_3 and $Gd_2O_3(Ga_2O_3)$, or on other substrates, such as *c*-plane sapphire, for which tilt and twist angles invariably exhibit the same trend of increase or decrease

Table 1 Lattice parameter, coherent length, inhomogeneous strain, tilt angle, twist angle, screw TD density and edge TD density of ZnO epi-layers grown at various temperatures

Growth temp.	Lattice constant (a) a and (b) c/Å	Coherent length (a) Surface-normal and (b) in-plane/Å	Inhomogeneous strain [$\times 10^{-3}$] (a) and surface-normal and (b) in-plane	Tilt angle/deg	Twist angle/deg	Edge TD density [$\times 10^{10}$ cm^{-2}] (a) and random and (b) pile up	Screw TD density [$\times 10^{9}$ cm^{-2}]
200 °C	3.26078	2341.36	1.63	0.419	1.636	17.64	4.56
	5.19273	2160.72	3.86			1.39	
300 °C	3.25384	2242.53	1.31	0.34	1.891	20	2.97
	5.19375	997.04	3.356			3.49	
400 °C	3.26055	1379.78	1.49	0.507	1.723	19.575	6.7
	5.19214	2720.39	4.69			1.64	

with growth conditions.[16] This result indicates that the tilt angle alone is insufficient to describe the crystalline quality of the ZnO films; one must take both tilt and twist angles into account.[16,29] Moreover, the opposite trend, increase and decrease, of the tilt and twist angles with growth conditions observed in this case allows us to examine independently the influence of edge and screw TDs on the optical and electrical properties of the grown films.

The TD density can be quantitatively estimated from the tilt or twist angle and the corresponding Burgers vector. The density of screw dislocations (N_s) is obtained with equation $N_S = \alpha_\Omega^2/4.35b_C^2$, in which α_Ω denotes the tilt angle and b_C is the length of the corresponding Burgers vector $\boldsymbol{b}_C$, which is [0001] with $b_C = 0.519$ nm in our case.[30] The edge TD density, N_E, is calculated from $N_E = \alpha_\Phi^2/4.35b_E^2$, in which α_Φ and b_E are the twist angle and the length of the corresponding Burgers vector ($b_E = 0.325$ nm), respectively, provided that the TDs follow a random distribution. If dislocations are piled up at small angle boundaries, the formula $N_E = \alpha_\Phi/2.1|b_E|L$ applies, in which the formation of subgrains of average size L along the lateral direction is taken into account. For a system with neither random nor piled-up distribution, the edge dislocation density lies between the two values. The calculated TD densities are also summarized in Table 1. The TD density estimated from the TEM contrast analysis is nearer that obtained with the piled-up model, which we thus adopt for subsequent correlation of structural and optical properties. As the density of edge TDs is much larger than that of screw TDs, edge TDs are the dominant type of dislocations in ZnO grown on γ-Al_2O_3/Si(111), consistent with the TEM observation, and the same as for ZnO films grown on the commonly used substrate, c-plane sapphire.

PL spectra recorded at 15 K, as displayed in Fig. 5, were measured to examine the optical characteristics of the ZnO films. The spectra comprise two main features, the intense and narrow near band-edge (NBE) emission, centered at ~3.36 eV, and the broad deep-level emission (DLE) located at ~2.2 eV, which is generally attributed to point defects such as Zn interstitials or O vacancies.[31–33] Expanded spectra of the NBE region with the spectrum of a ZnO wafer are shown in the inset. The dominant feature in the NBE region is assigned to the recombination of an A-exciton bound to a neutral donor (D^oX_A), of which the line position shifts toward smaller energy relative to that of strain-free bulk ZnO (3.366 eV). The extent of the red shift monotonically increases with the biaxial relaxation coefficient, $R^B = -\varepsilon_{zz}/\varepsilon_{xx}$, in which ε_{zz} and ε_{xx} denote the normal and lateral strains,[34] of the tensile-stressed ZnO layer; this phenomenon is similar to that reported for a GaN epi-layer.[35,36] The NBE spectrum of the sample grown at 300 °C is plotted on a semi-log scale in Fig. 6. Features associated with the longitudinal optical (LO) phonon replicas coupled with a donor-bound exciton D^oX_A, D^oX_A-1LO and D^oX_A-2LO, are centered at 3.288 eV and 3.215 eV, respectively. Other features, such as a two-electron satellite (TES) at 3.328 eV, a donor–acceptor pair (DAP) at 3.23 eV, and a free exciton FX_A at 3.375 eV are clearly identified, indicating the satisfactory optical properties of the obtained layers. By fitting the temperature-dependent intensity variation of the FX_A emission with an Arrhenius expression, we calculated an A-exciton binding energy to be 57.67 meV, in satisfactory agreement with 60 meV for bulk ZnO crystal.[1]

In addition to a narrow and intense NBE emission, a negligible DLE intensity is also desirable for optical applications. The intensity ratio of DLE to NBE emissions can be adopted as a measure of optical performance. The FWHM of NBE emissions and the ratio I_{DLE}/I_{NBE} for ZnO films grown at various temperatures are summarized in Table 2. The optical performance of a ZnO film grown at 300 °C is the best in the NBE region but the worst in the DLE region; *i.e.*, there exists an opposite trend between the NBE width and the ratio I_{DLE}/I_{NBE} with ZnO growth temperature. As mentioned above, the tilt and twist angles, which are, respectively, related to the density of edge- and screw-type TDs, also exhibit opposite trends with

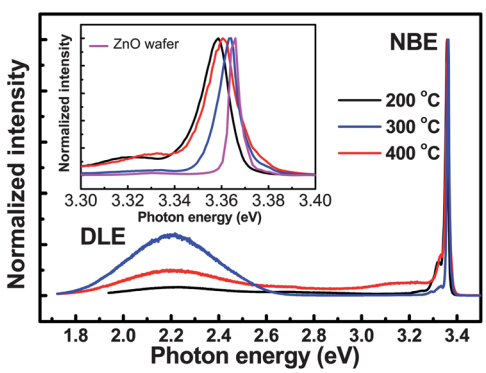

Fig. 5 PL spectra measured at 15 K for ZnO films grown at various temperatures. The intensities of the spectra are normalized to the maximum intensity of the NBE emission. The inset shows the NBE region spectra in magnification with the additional spectrum of bulk ZnO as a reference.

This journal is © The Royal Society of Chemistry 2012

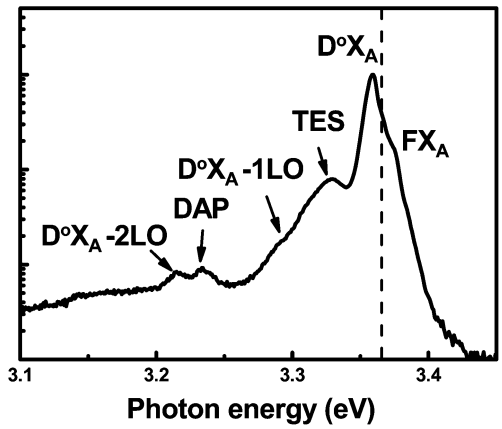

Fig. 6 NBE PL spectrum, measured at 15 K, of a sample grown at 300 °C. The dashed lines mark the position of the D^oX_A peak of bulk ZnO.

growth temperature. Fig. 7(a) shows the dependence of ratio I_{DLE}/I_{NBE} on the edge TD density calculated with the piled-up model. Fig. 7(b) illustrates the NBE line width as a function of screw TD density. The ratio I_{DLE}/I_{NBE} and the FWHM of the NBE exhibit a monotonic increase with the density of edge and screw TDs, respectively. In contrast, the distribution of I_{DLE}/I_{NBE} scatters randomly with the screw TD density, and the line width of the NBE emission shows no clear correlation with the edge TD density. The NBE emission is governed predominantly by the screw component of the TD, and the edge TDs play the key role in affecting the DLE intensity. This correlation between the structural quality and the optical performance is extensible to the ZnO epi-layers grown under similar conditions on *c*-plane sapphire, for which both the tilt angle, 0.17°, and the twist angle, 0.59°, of the ZnO layer are much smaller. Relative to ZnO grown on γ-Al_2O_3, it yields much smaller NBE line width, 7.03 meV, and a significantly smaller ratio, $I_{DLE}/I_{NBE} = 0.003$. The features in the NBE region, such as the longitudinal optical phonon replicas and DAP, were also better resolved in the layer grown on sapphire.

Similar phenomena have been reported for III-nitride epi-films, which have the same wurtzite structure and optical characteristics similar to those of ZnO. Zhao *et al.* reported that the intensity ratio of yellow to NBE luminescence of GaN epi-films depended strongly on the twist angle (screw dislocation density) and was much less influenced by the tilt angle (edge dislocation density).[36] That the FWHM of the PL NBE emission increases with screw dislocation density was reported also for AlN epi-layers.[37] All these observations support the arguments that screw

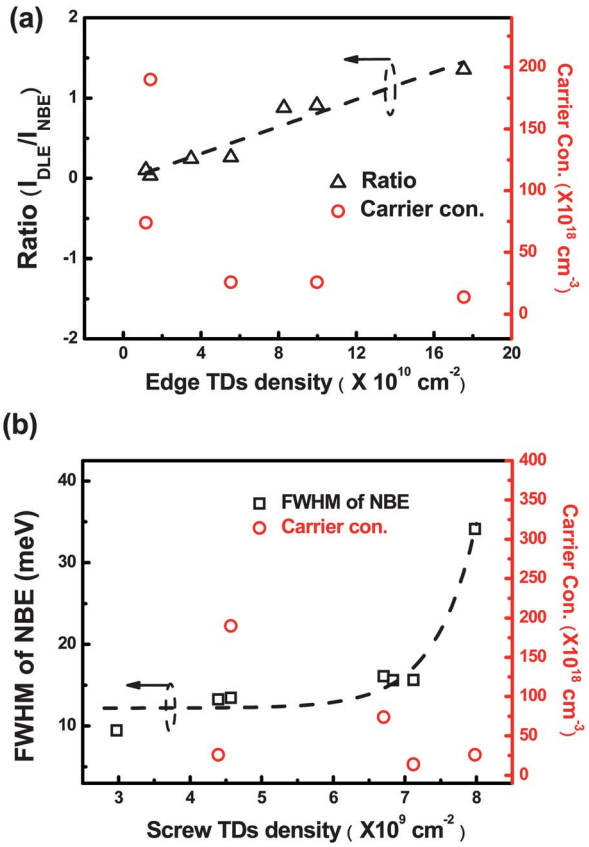

Fig. 7 (a) Ratio I_{DLE}/I_{NBE} and carrier concentration as a function of edge TD density. (b) Dependence of the NBE line width on the screw TD density. The dashed curves are plotted for visual guidance.

TDs can act as non-radiative centers in decreasing the NBE emission intensity, and the existence of edge TDs leads to aggregation of point defects due to the stress field near dislocation cores and results in an enhanced DLE intensity.[32,38]

We tested also the effect of post-growth annealing on the optical characteristics of the ZnO layers. After annealing at 800 °C for 100 min in an O_2 atmosphere, both the DLE emission intensity and the NBE line width diminished significantly. PL spectra of the sample grown at 300 °C, illustrated in Fig. 8, represent the typical effect of thermal annealing under O_2. The characteristic features of PL spectra before and after this thermal treatment are summarized in Table 2. In contrast, the DLE intensity was enhanced when the sample was annealed in a N_2 atmosphere. The structural quality of the films as characterized by XRD shows no obvious improvement after annealing. These tests indicate that O vacancies, to which XRD is insensitive, are plausibly another major source of DLE emission. According to

Table 2 Characteristic features, ratio I_{DLE}/I_{NBE} and NBE FWHM of PL spectra recorded for samples grown at various temperatures. Both as-deposited and after post-growth annealing data are included

	As deposited		Annealed	
Growth temp.	Ratio (I_{DLE}/I_{NBE})	NBE FWHM/meV	Ratio (I_{DLE}/I_{NBE})	NBE FWHM/meV
200 °C	0.033	13.44	0.0279	7.22
300 °C	0.244	9.44	0.0273	7.21
400 °C	0.101	16.09	0.0151	8.16

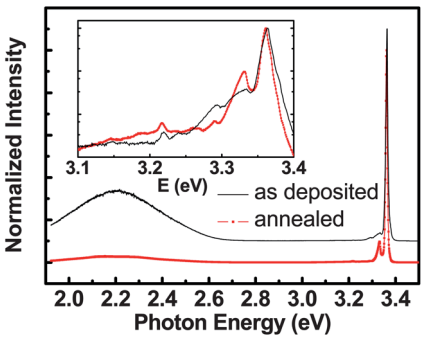

Fig. 8 PL spectra of a sample grown at 300 °C before and after thermal annealing in an O_2 atmosphere. Magnified NBE spectra are shown in the inset.

these results, we learned that both edge TD and O vacancies are intimately related to DLE; as for the correlation between edge TD and O vacancies, further tests are necessary to answer the question.

The electric properties of the ZnO films were characterized with measurements of the Hall effect conducted near 295 K. The major carriers in ZnO layers are verified to be electrons, revealing the n-type nature of the ZnO layers, the same as for typical undoped ZnO. The order of the obtained mobility is a few tens of $cm^2\ V^{-1}\ s^{-1}$. No obvious correlation between the carrier mobility and the density of edge or screw TDs was found. Also plotted in Fig. 7(a) and (b) are net carrier concentration *vs.* the edge and screw TD densities, respectively. The measured net carrier concentration decreases with increasing edge TD density but distributes randomly with screw TD density. The same phenomenon was reported by Zhao *et al.* on GaN grown on *c*-plane sapphire by MOCVD, for which the carrier concentration decreased with increasing XRD peak width of the GaN $(10\bar{1}2)$ reflection, or equivalently the density of edge TDs.[36,39] There exist many dangling bonds in the core of edge dislocation lines, in which impurities or point defects might be trapped. This condition would induce deep acceptor-like trap states that can capture electrons from the conduction band in n-type semiconductors and act as electron killers.[40,41] In the case of n-type GaN, the edge dislocation cores are normally negatively charged,[42] and the decreased concentration of free electrons can be attributed to the compensation effect from the increasing acceptor-like trap states introduced by the edge dislocations. In our previous work, results from a scanning capacitance microscope and a conductive atomic-force microscope (CAFM) indicated a smaller local carrier concentration and greater interface trap density, D_{it}, in the grain-boundary regions with a large density of negatively charged edge TDs in ZnO grown on *c*-plane sapphire.[13,15,43] First-principles studies on the energetics as well as atomic and electronic structures of native point defects in ZnO based on density functional theory within the local density approximation (LDA) and with additional Habbard U correction, LDA + U,[44,45] or within the generalized gradient approximation (GGA) and GGA + U,[45] both revealed that Zn vacancies with two negative charges, V_{Zn}^{2-}, have the lowest formation energy among all native point defects in n-type ZnO and exist in modest concentration. These acceptor-type defects can compensate for carrier electrons and result in the smaller local carrier concentration. It is thus plausible that doubly charged Zn vacancies (V_{Zn}^{2-}) are the defects trapped in the dislocation cores. In our previous CAFM studies, the local current–voltage (I–V) characteristics measured near the grain boundary with large density of TDs revealed the existence of a defect level of 0.4 ± 0.025 eV below the conduction band maximum. This defect level is in good agreement with the estimated V_{Zn}^{2-} energy level of 0.4–0.5 eV reported in ref. 46 and supports the above-mentioned argument. The V_{Zn}^{2-} decorated edge TDs thus play an important role in reducing the carrier concentration in n-type ZnO films.

Conclusions

A high-quality ZnO epitaxial film has been grown with pulsed-laser deposition on Si(111) substrates with a thin oxide γ-Al_2O_3 buffer layer. According to XRD and TEM analysis, the major defect structures in the ZnO film are threading dislocations; the edge type of TD is the dominant component in ZnO epi-films. The correlation between type of TD and their influence on optical and electrical properties was established with XRD, LT-PL and Hall measurements. Our results demonstrate that the ratio I_{DLE}/I_{NBE} and the carrier concentration are affected mainly by the edge TD, and the FWHM of the NBE is dominantly influenced by the screw TD. O vacancies also play an important role in affecting the DLE. The correlation between structure and other physical properties indicates that the edge type TD is more harmful to the optical and electric properties of ZnO than the screw type TD. To optimize growth parameters of ZnO or to develop a new growth method to effectively diminish the density of TDs, especially the edge-type ones, remains an important issue for its prospective applications to photonic devices.

Acknowledgements

We thank Professor S. Gwo and Dr H. M. Lee of Department of Physics, National Tsing Hua University, for assistance in the Hall measurements. National Science Council of Taiwan partly supported this work under grants NSC-96-2113-M-007-025-MY2 and NSC-97-2112-M-213-003-MY3.

References

1 D. M. Bagnall, Y. F. Chen, Z. Zhu, T. Yao, M. Y. Shen and T. Goto, *Appl. Phys. Lett.*, 1998, **73**, 1038.
2 Y. Z. Yoo, T. Sekiguchi, T. Chikyow, M. Kawasaki, T. Onuma, S. F. Chichibu, J. H. Song and H. Koinuma, *Appl. Phys. Lett.*, 2004, **84**, 502.
3 C. C. Lin, S. Y. Chen, S. Y. Cheng and H. Y. Lee, *Appl. Phys. Lett.*, 2004, **84**, 5040.
4 H. M. Cheng, H. C. Hsu, S. Yang, C. Y. Wu, Y. C. Lee, L. J. Lin and W. F. Hsieh, *Nanotechnology*, 2005, **16**, 2882.
5 W.-R. Liu, Y. H. Li, W. F. Hsieh, C.-H. Hsu, W. C. Lee, M. Hong and J. Kwo, *J. Phys. D: Appl. Phys.*, 2008, **41**, 065105.
6 W.-R. Liu, Y. H. Li, W. F. Hsieh, C.-H. Hsu, W. C. Lee, Y. J. Lee, M. Hong and J. Kwo, *Cryst. Growth Des.*, 2009, **9**, 239.
7 M. Fujita, N. Kawamoto, M. Sasajima and Y. Horikoshi, *J. Vac. Sci. Technol., B*, 2004, **22**, 1484.
8 X. N. Wang, Y. Wang, Z. X. Mei, J. Dong, Z. Q. Zeng, H. T. Yuan, T. C. Zhang, X. L. Du, J. F. Jia, Q. K. Xue, X. N. Zhang, Z. Zhang, Z. F. Li and W. Lu, *Appl. Phys. Lett.*, 2007, **90**, 151912.
9 W. Guo, M. B. Katz, C. T. Nelson, T. Heeg, D. G. Schlom, B. Liu, Y. Che and X. Q. Pan, *Appl. Phys. Lett.*, 2009, **94**, 122107.

 This journal is © The Royal Society of Chemistry 2012

10 N. Oleynik, A. Dadgar, J. Bläsing, M. Adam, A. Krtschil, D. Forster, F. Bertram, A. Diez, M. Seip, A. Greiling, J. Christen and A. Krost, *Jpn. J. Appl. Phys.*, 2003, **42**, 7474.
11 D. G. Zhao, D. S. Jiang, H. Yang, J. J. Zhu, Z. S. Liu, S. M. Zhang, J. W. Liang, X. Li, X. Y. Li and H. M. Gong, *Appl. Phys. Lett.*, 2006, **88**, 241917.
12 J. H. You and H. T. Johnson, *J. Appl. Phys.*, 2007, **101**, 023516.
13 W.-R. Liu, W. F. Hsieh, C.-H. Hsu, K. S. Liang and F. S.-S. Chien, *J. Cryst. Growth*, 2006, **297**, 294.
14 H. Alexander and H. Teichler, in *Materials Science and Technology, Electronic Structure and Properties of Semiconductor*, ed. W. Schröter, VCH, Weinheim, 1991, vol. 4, pp. 249–319.
15 W.-R. Liu, W. F. Hsieh, C.-H. Hsu, K. S. Liang and F. S.-S. Chien, *J. Appl. Crystallogr.*, 2007, **40**, 924.
16 M. Hong, M. Passlack, J. P. Mannaerts, J. Kwo, S. N. G. Chu, N. Moriya, S. Y. Hou and V. J. Fratello, *J. Vac. Sci. Technol., B*, 1996, **14**, 2297.
17 S. Y. Wu, M. Hong, A. R. Kortan, J. Kwo, J. P. Mannaerts, W. C. Lee and Y. L. Huang, *Appl. Phys. Lett.*, 2005, **87**, 091908.
18 J. Narayan and B. C. Larson, *J. Appl. Phys.*, 2003, **93**, 278.
19 B. H. Lin, W. R. Liu, S. Yang, C. C. Kuo, C.-H. Hsu, W. F. Hsieh, W. C. Lee, Y. J. Lee, M. Hong and J. Kwo, *Cryst. Growth Des.*, 2011, **11**, 2846.
20 W. Guo, A. Allenic, Y. B. Chen, X. Q. Pan, W. Tian, C. Adamo and D. G. Schlom, *Appl. Phys. Lett.*, 2008, **92**, 072101.
21 S. H. Lim, J. Washburn, Z. Liliental-Weber and D. Shindo, *J. Vac. Sci. Technol., A*, 2001, **19**, 2601.
22 F. Vigué, P. Vennéguès, S. Vézian, M. Laügt and J.-P. Faürie, *Appl. Phys. Lett.*, 2001, **79**, 194.
23 A. Howie and M. J. Whelan, *Proc. R. Soc. London, Ser. A*, 1962, **267**, 206.
24 A. C. McLaren, *Transmission Electron Microscopy of Minerals and Rocks*, Cambridge University, Cambridge, 1991, p. 387.
25 F. A. Ponce, in *Group III Nitride Semiconductor Compounds: Physics and Applications*, ed. B. Gil, Clarendon, Oxford, 1998, pp. 123–157.
26 R. Chierchia, T. Böttcher, H. Heinke, S. Einfeldt, S. Figge and D. Hommel, *J. Appl. Phys.*, 2003, **93**, 8918.
27 V. Srikant, J. S. Speck and D. R. Clarke, *J. Appl. Phys.*, 1997, **82**, 4286.
28 G. K. Williamson and W. H. Hall, *Acta Metall.*, 1953, **1**, 22.
29 T. Metzger, R. Hopler, E. Born, O. Ambacher, M. Stutzmann, R. Stommer, M. Schuster, H. Gobel, S. Christiansen, M. Albrecht and H. P. Strunk, *Philos. Mag. A*, 1998, **77**, 1013.
30 B. P. Zhang, Y. Segawa, K. Wakatsuki, Y. Kashiwaba and K. Haga, *Appl. Phys. Lett.*, 2001, **79**, 3953.
31 A. Teke, Ü. Özgür, S. Doğan, X. Gu, H. Morkoç, B. Nemeth, J. Nause and H. O. Everitt, *Phys. Rev. B: Condens. Matter Mater. Phys.*, 2004, **70**, 195207.
32 Y. F. Chen, D. M. Bagnall, H. J. Koh, K. T. Park, K. Hiraga, Z. Zhu and T. Yao, *J. Appl. Phys.*, 1998, **84**, 3912.
33 T. Onuma, S. F. Chichibu, A. Uedono, Y. Z. Yoo, T. Chikyow, T. Sota, M. Kawasaki and H. Koinuma, *Appl. Phys. Lett.*, 2004, **85**, 5586.
34 Y. F. Li, B. Yao, Y. M. Lu, C. X. Cong, Z. Z. Zhang, Y. Q. Gai, C. J. Zheng, B. H. Li, Z. P. Wei, D. Z. Shen, X. W. Fan, L. Xiao, S. C. Xu and U. Liu, *Appl. Phys. Lett.*, 2007, **91**, 021915.
35 D. G. Zhao, S. J. Xu, M. H. Xie, S. Y. Tong and H. Yang, *Appl. Phys. Lett.*, 2003, **83**, 677.
36 D. G. Zhao, D. S. Jiang, H. Yang, J. J. Zhu, Z. S. Liu, S. M. Zhang, J. W. Liang, X. Li, X. Y. Li and H. M. Gong, *Appl. Phys. Lett.*, 2006, **88**, 241917.
37 B. N. Pantha, A. Sedhain, J. Li, J. Y. Lin and H. X. Jiang, *Appl. Phys. Lett.*, 2010, **96**, 131906.
38 U. Bangert, A. J. Harvey, R. Jones, C. J. Fall, A. Blumenau, R. Briddon, M. Schreck and F. Hörmann, *New J. Phys.*, 2004, **6**, 184.
39 D. G. Zhao, H. Yang, J. J. Zhu, D. S. Jiang, Z. S. Liu, S. M. Zhang, Y. T. Wang and J. W. Liang, *Appl. Phys. Lett.*, 2006, **89**, 112106.
40 W. T. Read, *Philos. Mag.*, 1954, **45**, 775.
41 B. Pödör, *Phys. Status Solidi B*, 1966, **16**, K167.
42 K. Leung, A. F. Wright and E. B. Stechel, *Appl. Phys. Lett.*, 1999, **74**, 2495.
43 C. Y. Lin, W.-R. Liu, C. S. Chang, C.-H. Hsu, W. F. Hsieh and F. S.-S. Chien, *J. Electrochem. Soc.*, 2010, **157**, H268.
44 A. Janotti and C. G. Van de Walle, *Phys. Rev. B: Condens. Matter Mater. Phys.*, 2007, **76**, 165202.
45 F. Oba, M. Choi, A. Togo and I. Tanaka, *Sci. Technol. Adv. Mater.*, 2011, **12**, 034302.
46 F. A. Kröger, in *The Chemistry of Imperfect Crystal. Imperfection Chemistry of Crystalline Solids*, North-Holland, Amsterdam, 2nd edn, 1974, vol. 2.